THE JOURNAL OF BIOLOGICAL CHEMISTRY VOL. 287, NO. 44, pp. 37483–37494, October 26, 2012

Pharmacological Modulation of the Retinal Unfolded Protein Response in Bardet-Biedl Syndrome Reduces Apoptosis and Preserves Light Detection Ability*[S]

Received for publication, June 1, 2012, and in revised form, July 24, 2012 Published, JBC Papers in Press, August 6, 2012, DOI 10.1074/jbc.M112.386821

Anais Mockel[‡], Cathy Obringer[‡], Theodorus B. M. Hakvoort[§], Mathias Seeliger[¶], Wouter H. Lamers[§], Corinne Stoetzel[¶], Hélène Dollfus[‡‖], and Vincent Marion[‡1]

From the [‡]Laboratoire de Physiopathologie des Syndromes Rares Héréditaires, AVENIR-INSERM, EA3949, Université de Strasbourg, 67085 Strasbourg, France, the [§]Tytgat Institute for Liver and Intestinal Research, Academic Medical Center, University of Amsterdam, 1100 DD, Amsterdam, The Netherlands, the [¶]Division of Ocular Neurodegeneration, Center for Ophthalmology, Institute for Ophthalmic Research, D-72076 Tübingen, Germany, and the [‖]Service de Génétique Médicale, Hôpitaux Universitaires de Strasbourg, 67200 Strasbourg, France

Background: Retinal degeneration is a main feature of Bardet-Biedl syndrome for which the mechanism causing photoreceptor cell apoptosis remains elusive.
Results: Apoptosis is caused by protein accumulation in the photoreceptor inner segment activating an unfolded protein response.
Conclusion: Pharmacological reduction of apoptosis preserves light detection ability.
Significance: This therapeutic approach could be used to slow the degeneration and is potentially applicable to other ciliopathies.

Ciliopathies, a class of rare genetic disorders, present often with retinal degeneration caused by protein transport defects between the inner segment and the outer segment of the photoreceptors. Bardet-Biedl syndrome is one such ciliopathy, genetically heterogeneous with 17 BBS genes identified to date, presenting early onset retinitis pigmentosa. By investigating BBS12-deprived retinal explants and the *Bbs12*$^{-/-}$ murine model, we show that the impaired intraciliary transport results in protein retention in the endoplasmic reticulum. The protein overload activates a proapoptotic unfolded protein response leading to a specific Caspase12-mediated death of the photoreceptors. Having identified a therapeutic window in the early postnatal retinal development and through optimized pharmacological modulation of the unfolded protein response, combining three specific compounds, namely valproic acid, guanabenz, and a specific Caspase12 inhibitor, achieved efficient photoreceptor protection, thereby maintaining light detection ability *in vivo*.

Bardet-Biedl syndrome (BBS, Online Mendelion Inheritance in Man 290900)[2] is characterized by early onset retinitis pigmentosa (RP), polydactyly, obesity, renal dysfunction, hypogonadism, and cognitive impairment (1). It is an emblematic member of the ciliopathies, a group of inherited genetic diseases caused by a defect in the primary cilium organelle (2). BBS is a genetically heterogeneous condition with at least 17 genes identified so far (*BBS1–BBS17)* (3). The BBS proteins are localized within the primary cilium-centrosome complex and are involved in the biogenesis and/or function of the primary cilium (4). Functionally, seven BBS proteins (BBS1, 2, 4, 5, 7, 8, and 9) form a stable complex named the BBSome and are involved in ciliary transport of specific cargo proteins (5). The BBSome assembly is dependent of a second BBS complex, a chaperone complex including BBS6, 10, and 12 (6). Because of the strong functional interactions between these BBS proteins, the loss of one of these proteins impairs the proper functioning of the ciliary complex and leads to the disabling clinical manifestations that characterize BBS.

Retinal degeneration in BBS is thought to be due to a defect in intraciliary transport (ICT) in the connecting cilium of the photoreceptor (7). The latter is a modified primary cilium that links the biosynthetically active inner segment (IS) to the light-sensitive outer segment (OS) (2). BBS-mediated impairment of the ICT causes a slow process of degeneration eventually causing the total loss of the photoreceptors (8–12). Retinal phenotyping in the reported BBS mouse models has, indeed, shown that apoptosis correlated with an impaired ICT of major photoreceptor proteins like Rhodopsin and Arrestin (7). Interestingly, it was also shown that mutated forms of Rhodopsin accumulate in the IS and trigger apoptosis (13), which is reminiscent of the phenotype observed in several ciliopathies that also cause pro-

* This work was supported by the Agence Nationale pour la Recherche (ANR Call for Rare Diseases 2009) and the INSERM Avenir Program.
[S] This article contains supplemental text and Figs. S1–S14.
[1] To whom correspondence should be addressed: National Institute for Health and Medical Research (INSERM), Laboratoire de Physiopathologie des Syndromes Rares Héréditaires, University of Strasbourg, Faculty of Medicine, 9th Floor, Bldg. 3, 11 Rue Humann, 67085 Strasbourg cedex, France. Tel: 33-3-68-85-33-34; Fax: 33-3-68-85-31-10; E-mail: vincent.marion@unistra.fr.
[2] The abbreviations used are: BBS, Bardet-Biedl syndrome; ICT, intra-ciliary transport; RP, retinitis pigmentosa; ER, endoplasmic reticulum; UPR, unfolded protein response; BiP, immunoglobulin heavy chain-binding protein; eIF, eukaryotic initiation factor; HRI, heme-regulated inhibitor; OS, outer segment; IS, inner segment; ONL, outer nuclear layer; VPA, valproic acid; GBZ, guanabenz; INH, Caspase12 inhibitor; GIV, GBZ + VPA + INH; GIV*in*, GIV *in vivo*; ERG, electroretinogram.

tein overload in the IS (14). Protein accumulation is deleterious because it stresses the endoplasmic reticulum (ER). In an attempt to alleviate ER stress, the cell activates a series of coordinated cellular responses known as the unfolded protein response (UPR) (15). Unfortunately, when the UPR fails to restore cellular homeostasis, the UPR switches to a proapoptotic process. Other animal models of inherited RP are also linked to ER stress (16), such as the *rd1* mouse (17), and RP models linked to Rhodopsin mutations (18–20). Interestingly, therapeutic efforts to modulate the UPR in some RP models were efficient in protecting the photoreceptors against cell death (21, 22), but to date, none of them was able to maintain the ability of the retina to detect light.

In an attempt to prevent photoreceptor apoptosis in BBS, we studied the UPR signaling cascade in BBS12-deficient retinal explants and the corresponding *Bbs12* knock-out mouse model (*Bbs12*$^{-/-}$). BBS12 inactivation impaired ICT in the photoreceptors and triggered an activation of the UPR caused by protein accumulation in the IS. This UPR caused activation of Caspase12, which drove the apoptosis in the *Bbs12*-deprived photoreceptors. Interestingly, through a specific pharmacological modulation of the UPR to alleviate the ER stress, we were able to prevent apoptosis of the photoreceptor both *ex vivo* and *in vivo*, thereby maintaining light detection ability of the retina in the *Bbs12*$^{-/-}$ mouse.

EXPERIMENTAL PROCEDURES

Retinal Explants—Wild-type animals had a C57BL/6 background. Retinal explants were cultured as previously described (23). Briefly, 15-day-old mice were sacrificed by decapitation, and the eyes were removed and incubated for 10 min at 37 °C in a 10% trypsin solution (catalogue number 25200-072; Invitrogen). Digestion was stopped by transferring the eyes to DMEM with 10% fetal bovine serum (catalogue numbers 31885-023 and 10500-064; Invitrogen) and incubating them for 10 min at 4 °C. The eyes were dissected in Ames' medium (catalogue number 15230-097; Invitrogen) supplemented with 6.5 μg/liter glucose. First, the sclera was carefully removed, leaving the retinal pigmented epithelium attached to the eye ball. Incisions were made at the edge of the cornea to remove cornea, lens, and hyaloid body. Then four equidistant, radial incisions were made in the retina. The retinas were transferred, with retinal pigmented epithelium side down, to a nitrocellulose culture membrane (catalogue number PICMORG50; Millipore, Molsheim, France) and cultivated in Neurobasal A medium (catalogue number 108888-022; Invitrogen) supplemented with B27 (catalogue number 17504-044; Invitrogen), L-glutamine (catalogue number 35050-061; Invitrogen), and penicillin/streptomycin (catalogue number 15240; Invitrogen). Explants were maintained at 37 °C in a humidified 5% CO_2 atmosphere. Specific gene silencing with lentiviruses that carried a shRNA sequence for *Bbs12*, *Perk*, *Hri* (catalogue numbers sc-108080 (*Ctl*), sc-141483-V (*Bbs12*), sc-36214-V (*Perk*), and sc-39053-V (*Hri*); Santa Cruz Biotechnology, Tebu Bio, Yvelines, France) was performed by adding 20 μl of a viral suspension containing 10^5 infectious units to the culture medium overnight. The infected explants were then washed and cultured for 3 days, with half the medium refreshed daily. Explants were not maintained longer in culture to avoid unspecific apoptosis in the different retinal layers. For pharmacological treatments, 2 mM valproic acid (VPA dissolved in ethanol 100%; catalogue number 4543; Sigma-Aldrich), 25 μM guanabenz (GBZ dissolved in Me_2SO; catalogue number 0889; Tocris Bioscience, Ellisville, MO), or 10 μM Caspase12 inhibitor (named INH dissolved in Me_2SO, the synthetic peptide Z-Ala-Thr-Ala-Asp(*O*-methyl)-fluoromethyl-ketone; catalogue number PK-CA577-1079-100; Promokine, Heidelberg, Germany) were added for single treatments and at a 10-fold dilution for combined treatments: GIV (GBZ 2.5 μM + 1 μM INH + 0.2 mM VPA) or GV (2.5 μM GBZ + 0.2 mM VPA). Drugs were added simultaneously with viral infection to the culture medium.

Immunofluorescence and TUNEL Assay—For immunofluorescence and TUNEL assays, retinal explants were fixed directly on membranes with 4% buffered formaldehyde for 1 h at 4 °C. Sucrose was then impregnated by incubating for 20 min each in 10, 20, and 30% sucrose solutions. Explants were transferred to OCT-containing molds (catalogue number 4583; Tissue-Tek, Sakura, Villeneuve d'Ascq, France) and frozen in liquid nitrogen. Eight micrometer-thin cryosections were mounted on StarFrost slides (catalogue number VS1117; Waldemar Knittel Glasbearbeitungs, Braunschweig, Germany). Sections or cells were washed with 1× PBS, fixed for 5 min in 4% formaldehyde solution, and washed three times with 1× PBS. The sections were preincubated in Teng-T (10 mM Tris-HCl, pH 7.6, 5 mM EDTA (catalogue number E5768; Sigma-Aldrich), 150 mM NaCl, 0.25% gelatin (catalogue number G9391; Sigma-Aldrich), 0.05% Tween 20), and 10% normal goat serum (catalogue number PCN5000; Invitrogen)) for 30 min, followed by an overnight incubation with the primary antibody diluted in PBS with 5% BSA at 4 °C. The slides were then washed with 1× PBS and incubated with the indicated secondary antibody in PBS with 5% BSA for 1 h at room temperature. After washing in 1× PBS, nuclear staining was performed with DAPI (catalogue number D1306; Invitrogen). The slides were mounted with Immumount (catalogue number 9990402; ThermoFisher). The antibodies are listed in the supplemental text. The TUNEL assays were performed using an *in situ* cell death detection kit (catalogue number 11684795910; Roche Applied Science) according to the supplier's protocol. The prevalence of apoptotic nuclei was expressed as the ratio of TUNEL-positive nuclei and DAPI-stained nuclei in three different areas of the ONL per experiment. All results shown are representative of at least three separate experiments.

Light Adaptation Experiments—Light adaptation was tested at 37 °C on explants after 3 days of culture to allow gene knockdown. For dark to light transition experiments, the explants were dark-adapted for 4 h and then exposed to 200 lux for 30 min by light-emitting diodes. For light to dark transition experiments, the explants were exposed to 200 lux for 15 min before dark adaptation for 45 min. After treatment, the explants were fixed with 4% formaldehyde in the illumination condition used.

Bbs12$^{-/-}$ *Mice Breeding and Pharmacological Treatments*—The constitutive knock-out of *Bbs12* was performed to generated *Bbs12*$^{-/-}$ mice, as described elsewhere (60). *Bbs12*$^{-/-}$ mice were obtained by crossing heterozygous animals. The

mice were housed in humidity- and temperature-controlled rooms on a 12-h light/12-h dark cycle with food and water *ad libitum*. For systemic VPA or systemic GBZ administration, the drug was added to the drinking water at a concentration of 5 mg/ml and 50 μM, respectively. For GIV *in vivo* (GIV*in*) treatment, the animals were treated, in addition to the daily systemic administration of VPA, with eyedrops containing 7.5 μM GBZ and 500 μM Caspase12 inhibitor for the left eye and 5% Me_2SO for the right eye. Eyedrop treatment was given between 2 and 4 weeks of age, and systemic treatment was given between 3 and 4 weeks of age. At 4 weeks of age, electrophysiological analyses were performed, and the retinas were harvested for molecular analysis.

Electroretinograms—The mice were dark adapted for 12 h prior to recording. The experiments were carried out in dim red light (catalogue number R125IRR; Philips, Suresnes, France). The mice were anesthetized by injecting them with 25 μl/10 g of body weight of a mix containing 100 μl of Domitor (Domitor 1 mg/ml; Janssen-Cilag, Issy-les-Moulineaux, France), 314 μl of Ketamine (Ketamine 1000; Virbac, Carros, France), and 4 ml of 0.9% NaCl. The pupils were dilated with 0.3% atropine eyedrops (Atropine Alcon 0.3%; Alcon, Rueil-Malmaison, France). The animals were placed on a heating pad and kept at 37 °C during the procedure. The reference electrode was placed under the head skin, and the background electrode was inserted into the tail of the animal. The measuring electrode was placed on the cornea. To optimize contact between the cornea and the gold electrode, a drop of methylcellulose gel (Ocry-gel; TVM Laboratories, Lempdes, France) was added. Flashes were delivered though a Ganzfeld lamp equipped with light-emitted diodes with a maximum output of 318 cd/m^2 (Siem Biomédicale, Nimes, France). For the scotopic electroretinograms, the flash duration varied from 3 to 5 ms, with the final flash output ranging from 0.001 to 1 cd*s/m^2. Responses were amplified, filtered (1–300-Hz band pass), and digitized (Visiosystem; Siem Biomédicale). The *a* and *b* waves were measured by using a 1–75-Hz band pass to filter oscillatory potentials.

RESULTS

Bbs12 Depletion in Retinal Explants Leads to Photoreceptor Abnormalities and Impaired ICT—To investigate the impact of *Bbs12* deprivation in the photoreceptors, we developed an *ex vivo* organotypic model of retinal explants that maintained retinal organization and photoreceptors integrity (supplemental Fig. S1) (23). *Bbs12* shRNA-mediated depletion resulted in a significant reduction of *Bbs12* mRNA expression levels (Fig. 1*A*) and an even stronger reduction in BBS12 protein content in the treated retinal explants (Fig. 1*B*). Subsequent histological studies showed general disorganization of photoreceptors (Fig. 1*C*) and dilatation of disks in the OS of the photoreceptors (Fig. 1*D*). ICT defects were also detected because we could observe Rhodopsin accumulation in the IS and the absence of Arrestin transport in the OS upon photonic stimulation (Fig. 1, *E* and *F*).

Apoptotic Phenotype and Mechanism in Bbs12-deprived Retinal Explants—To assess photoreceptor cell death after *Bbs12* inactivation, TUNEL assays were performed. A significant 3-fold increase in the number of apoptotic cells in the ONL of *Bbs12* shRNA-treated retinal explants was counted (Fig. 2*A* and supplemental Fig. S2). Measurement of the expression levels of the different Caspases mRNAs revealed significant up-regulation of the effector Caspase3, -6 and -7 (24) (Fig. 2*B*). The expression level of the Caspase9 activator, which is usually activated by a mitochondrial defect (25), remained unchanged, suggesting no mitochondrial involvement in the retinal phenotype of BBS. On the other hand, the expression level of activator Caspase12, which is activated by ER stress (26), was 2-fold higher in *Bbs12*-depleted explants.

As anticipated (27), the expression the ER chaperone BiP increased after knockdown of *Bbs12* (Fig. 2*B*). The ER-stress also induced ER-resident proteins IRE1 (inositol-requiring protein-1) and PERK (protein kinase RNA-like ER kinase, an ER-resident transmembrane kinase) activation. Both IRE1 and PERK act as sensors in the ER lumen and transmit information to the rest of the cell (28). Active IRE1 produces an alternative, shorter splice variant of the X-box-binding protein 1 (*Xbp1)* (29). The abundance of short *Xbp1* was indeed increased in the absence of BBS12 (Fig. 2*C*). Activation of PERK upon BBS12 deprivation was deduced from the increased phosphorylation of the eukaryotic initiation factor 2α (peIF2α) (30) (Fig. 2*D*). peIF2α inhibits CAP-dependent translation and, thus, decreases cellular protein load. peIF2α also increased the expression of *Chop10* (Fig. 2*B*) and increased the protein content of both BiP and CHOP10 (c/EBP-homologous protein 10; Fig. 2*D* and supplemental Fig. S2) in *Bbs12*-deprived retinal explants.

Together with PERK, three other stress kinases are able to phosphorylate eIF2α, namely heme-regulated inhibitor, PKR (double-stranded RNA-dependent protein kinase), and GCN2 (general control nonrepressed-2). GCN2 is activated in amino acid starvation and UV damage conditions (31), heme-regulated inhibitor during oxidative stress and heme deprivation (32), and PKR by viral infection (33). With the same viral antisense titers and culture conditions, we excluded a role for either PKR or GCN2 in the observed phenotype. Heme-regulated inhibitor kinase activity was excluded because simultaneous knockdown of *Bbs12* and *Hri* had no effect on the expression levels of the tested apoptotic genes nor altered the number of apoptotic nuclei in the corresponding retinal explants (supplemental Fig. S3). To verify that only PERK phosphorylated eIF2α in our experiments, we performed shRNA-mediated *Perk* knockdown in retinal explants (supplemental Fig. S4*A*) and show that it had no effect on the expression of the tested genes and number of apoptotic nuclei (Fig. 2, *E* and *F*). The simultaneous depletion of *Perk* and *Bbs12* caused, on the other hand, a significant reduction of the number of apoptotic nuclei in the ONL (Fig. 2*E* and supplemental Fig. S4*B*) and expression levels of *Caspase12*, *Chop10*, and *Bip* mRNAs (Fig. 2*F*).

Apoptosis of Photoreceptors Is Alleviated by Targeted Pharmacological Modulation of Key UPR Components—Modulating the activity of key UPR-related proteins protects against apoptosis (22, 34). Based on our findings, BiP, PERK-mediated phosphorylation of eIF2α and Caspase12 are key UPR actors in *Bbs12*-deprived photoreceptors phenotype. We therefore tried to modulate their activities to protect the *Bbs12*-depleted pho-

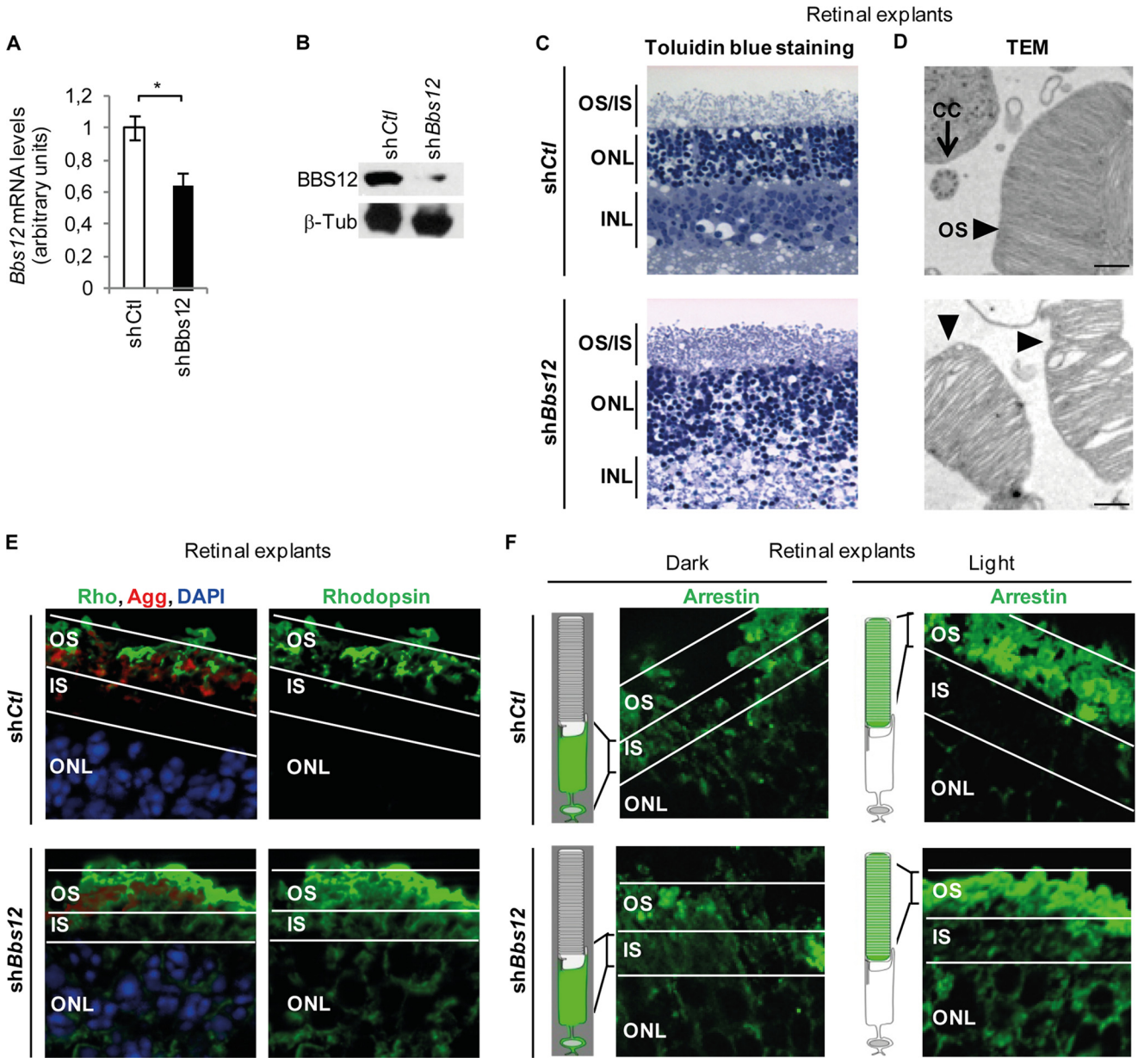

FIGURE 1. **Bbs12 depletion in retinal explants induces photoreceptor abnormalities.** *A*, *Bbs12* expression levels in indicated shRNA-treated explants 72 h after infection ($n = 3$). *shCtl*, control shRNA; *shBbs12*, *Bbs12*-shRNA. *, $p < 0.01$. *B*, immunodetection of BBS12 and β-tubulin as loading control in treated explants. *C*, toluidin blue-stained sections of treated explants. *Scale bars*, 50 μm. *INL*, inner nuclear layer. *D*, transmission electron microscopy (*TEM*) pictures showing photoreceptors OS and connecting cilium (*CC*) of sh*Ctl*-treated (*upper panel*) and sh*Bbs12*-treated (*lower panel*) explants. *Scale bars*, 500 nm. *E*, immunostaining of Rhodopsin with DAPI and OS counterstaining using Agglutinin in treated explants. *Scale bars*, 15 μm. *F*, immunostaining of Arrestin in dark-adapted (*left panel*) and in light-adapted (*right panel*) treated explants and schematic representation shows the expected localization of Arrestin under both conditions. *Scale bars*, 15 μm. See supplemental Fig. S1*C* for OS and ONL staining.

toreceptors with the use of three different compounds. Up-regulation of BiP was achieved by treating the explants with valproic acid (VPA) (35). Guanabenz (GBZ), an inhibitor of the eIF2α phosphatase GADD34, was used to maintain high levels of peIF2α and block CAP-dependent translation (36). Lastly, Caspase12 activity was repressed by treating the photoreceptors with a cell-permeable synthetic peptide (INH) that specifically blocks the catalytical site of the protease. In the absence of BBS12, 36, 18, 14, and 26% of the ONL nuclei in, respectively, untreated and VPA-, GBZ-, and INH-treated explants were apoptotic (Fig. 3*A*). Interestingly, the combination of VPA, GBZ, and INH in the GIV treatment was more efficient in decreasing apoptosis than any of the individual components of this combination at a 10-fold higher concentration. Indeed, the impact of *Bbs12* inactivation was completely balanced by the simultaneous pharmacological modulation of all three targets (Fig. 3*A* and supplemental Figs. S5 and S6). To understand how GIV could be the most efficient treatment in preventing photoreceptors apoptosis, we analyzed the level of targeted proteins (Fig. 3*B* and supplemental Fig. S7). VPA and GIV treatments maintained high BiP expression level in Ctl and BBS12-deprived retinas (Fig. 3*C*) and specifically in photoreceptors as validated by immunofluorescence (supplemental Fig. S8). GBZ and GIV caused an increase in the peIF2α levels, whereas VPA

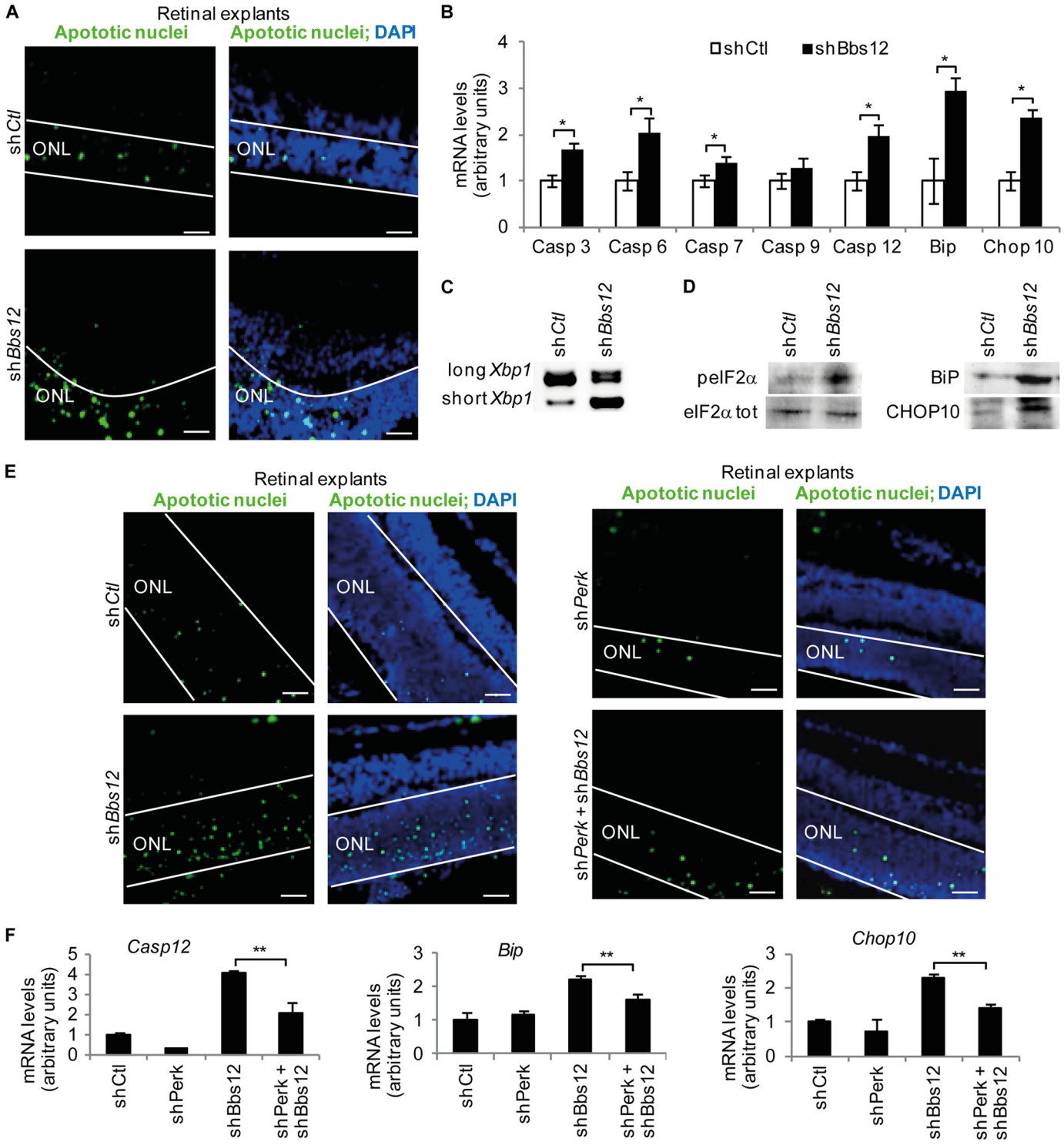

FIGURE 2. **Bbs12 depleted retinal explants present ER stress-mediated apoptosis.** *A*, TUNEL assays on indicated treated explants, 72 h after infection; apoptotic nuclei labeled in *green* and DAPI counterstaining. *Scale bars*, 25 μm. See supplemental Fig. S2*A* for corresponding apoptotic levels. *B*, expression analysis of *Caspase3*, *-6*, *-7*, *-9*, *-12*, *Bip*, and *Chop10* in treated explants ($n = 3$). *, $p < 0.01$. *C*, reverse transcription PCR of both long (unstressed) and short (unfolded protein response-related) forms of *Xbp1*. *D*, immunodetection of peIF2α, eIF2αtot, BiP, and CHOP10 in the indicated shRNA-treated explants. See supplemental Fig. S2 (*B–D*), for loading controls and quantification. *E*, TUNEL assays in sh*Ctl*, sh*Bbs12*, sh*Perk*, or sh*Bbs12* + sh*Perk*-treated explants. *Scale bars*, 25 μm. See supplemental Fig. S4 for corresponding apoptotic levels and *Perk* knockdown validation. *F*, expression analysis of *Caspase12*, *Bip*, and *Chop10* in indicated shRNA-treated explants ($n = 3$). **, $p < 0.05$.

decreased it (Fig. 3*D*). A significant increase of CHOP10 protein levels was observed by GBZ and GIV treatment. As expected, VPA decreased the concentration of CHOP10 (Fig. 3*E*). Surprisingly, the impact of INH on apoptosis correlated with a decrease in peIF2α and CHOP10. On the other hand, GIV treatment was the only treatment that successfully increased simultaneously BiP, peIF2α, and CHOP10 concentrations (Fig. 3, *C–E*). We next established that these GIV-me-

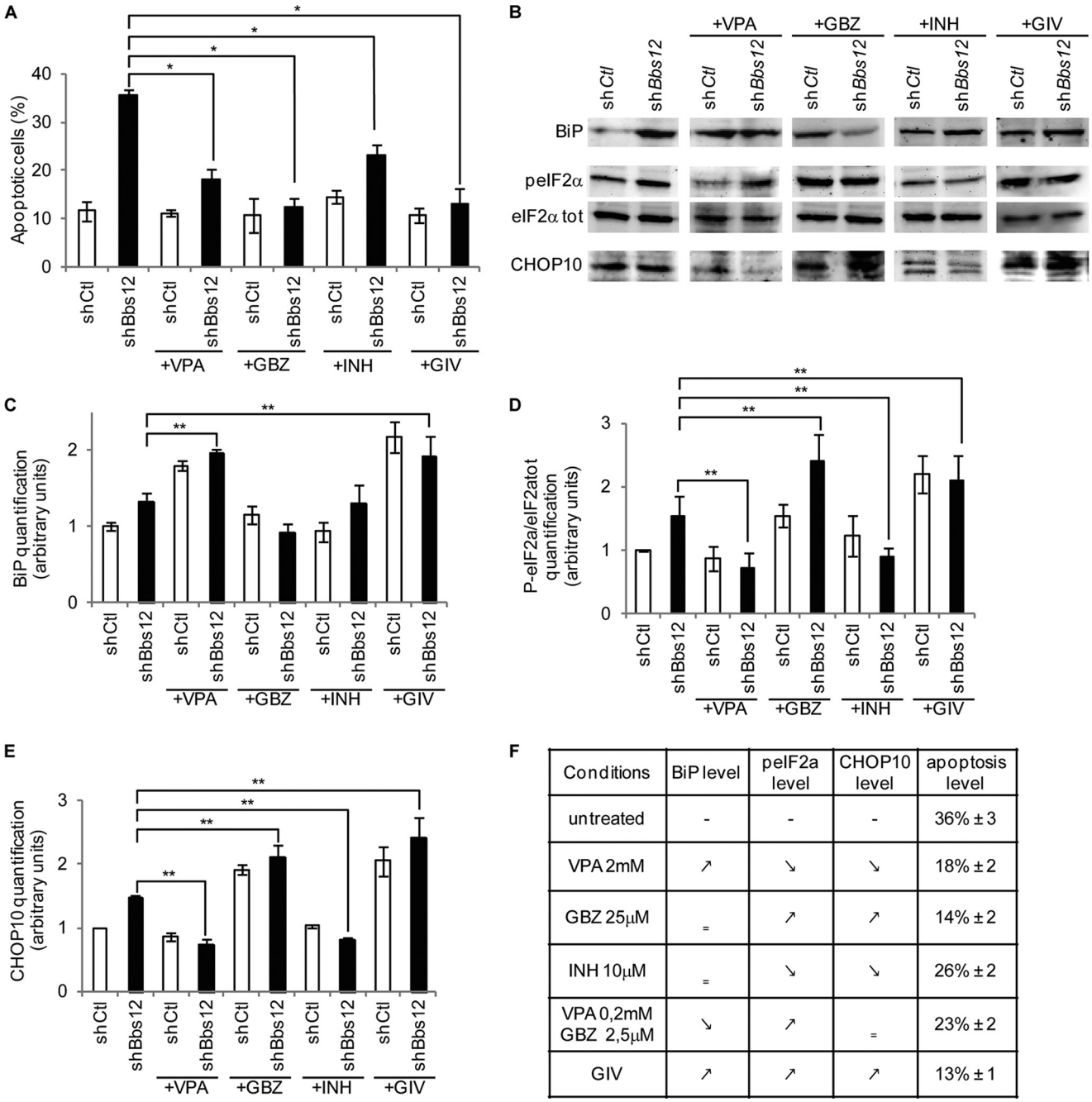

F

Conditions	BiP level	peIF2a level	CHOP10 level	apoptosis level
untreated	-	-	-	36% ± 3
VPA 2mM	↗	↘	↘	18% ± 2
GBZ 25μM	=	↗	↗	14% ± 2
INH 10μM	=	↘	↘	26% ± 2
VPA 0,2mM GBZ 2,5μM	↘	↗	=	23% ± 2
GIV	↗	↗	↗	13% ± 1

FIGURE 3. **Pharmacological modulation of UPR-related actors reduces apoptosis in *Bbs12*-depleted retinal explants.** *A*, effect on apoptotic levels of VPA or GBZ or INH or GIV treatments on sh*Ctl* and sh*Bbs12* explants (counted as TUNEL positive nuclei/DAPI in the ONL, $n = 3$). *, $p < 0.01$. See supplemental Figs. S5*A* and S6 for TUNEL assay. *B*, immunodetection of peIF2α, eIF2αtot, CHOP10, and BiP in the indicated shRNA-treated explants. See supplemental Fig. S7 for loading controls. *C–E*, quantification of peIF2α/tot, CHOP10, and BiP levels in the indicated shRNA-treated explants ($n = 3$). **, $p < 0.05$. *F*, table summarizing the effect of the different treatments on targeted proteins and apoptosis level (% ± S.E.). See supplemental Fig. S9 for VPA 0.2 mM + GBZ 2.5 μM treated explants.

diated protective effects were based on the synergistic action of all three compounds. The combination of GBZ and VPA (GV) did not increase all three targets and was therefore less protective against apoptosis (18% apoptotic nuclei for GV *versus* 13% for GIV; Fig. 3*F* and supplemental Fig. S9).

Retinal Phenotype of Bbs12$^{-/-}$ Mice—Histological studies in 4-week-old mice revealed a thinning of the retinal cell layers in *Bbs12*$^{-/-}$ mice (Fig. 4*A*) as exemplified by the measurement of the ONL (37 μm in *Bbs12*$^{-/-}$ retinas compared with 65 μm in *Bbs12*$^{+/+}$ retinas; Fig. 4*B*) and the drastic thinning of IS and OS. Transmission electron microscopy showed dilatation of disks inside the disrupted OS (Fig. 4*C*). Scotopic electroretinogram (ERG) recordings of these mice revealed a significant general decrease in the response to light stimuli, primarily linked to a substantial loss of the *a*-wave in *Bbs12*$^{-/-}$ mice (Fig. 4*D*, *red arrows*). The characteristic localization of Rhodopsin and Arrestin to the OS was lost in the *Bbs12*$^{-/-}$ mice (Fig. 4, *E* and *F*), which implies severe ICT defects in the *Bbs12*$^{-/-}$ retina. Finally, the massive accumulation of proteins in the IS resulted in swelling of the ER cisternae of the *Bbs12*$^{-/-}$ photoreceptors (Fig. 4*G*).

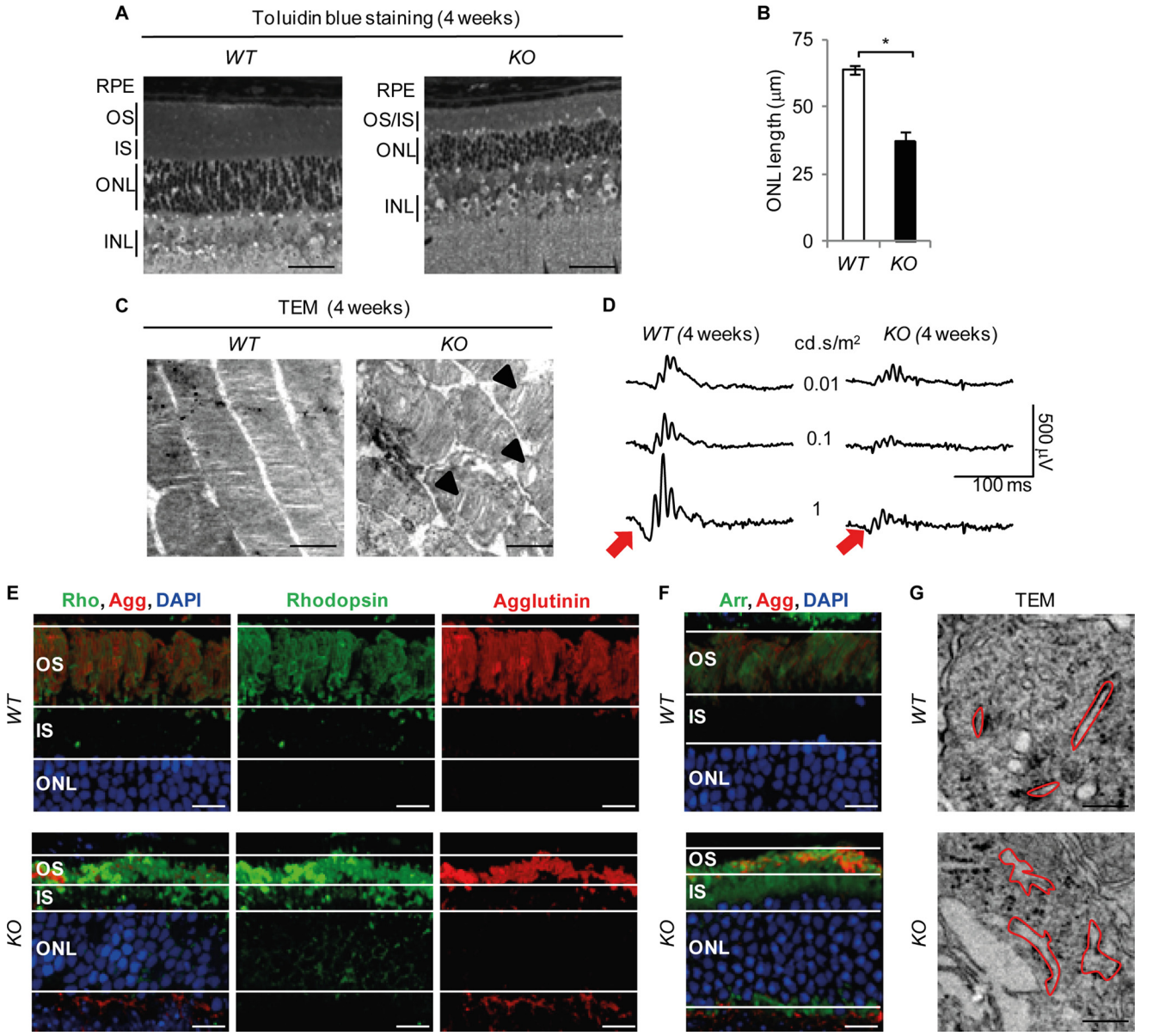

FIGURE 4. **Bbs12$^{-/-}$ mouse presents retinal degeneration.** *A*, toluidin blue-stained sections of the *WT* (*Bbs12*$^{+/+}$, *left panel*) and *KO* (*Bbs12*$^{-/-}$, *right panel*) retinas at 4 weeks of age. *Scale bars*, 50 μM. *B*, determination of ONL thickness of the *WT* and *KO* mice at 4 weeks ($n = 6$). *, $p < 0.01$. *C*, transmission electron microscopy (*TEM*) pictures of the outer segments of WT and KO retinas at 4 weeks. *Scale bars*, 1 μM. *Arrows* point to disk dilatation. *D*, scotopic ERG recordings for specified genotypes at 4 weeks. *Red arrows* present *a*-waves. *E* and *F*, immunostaining of Rhodopsin (*E*, *Rho*) and Arrestin (*Arr*, *F*) in *WT* and *KO* retinas at 4 weeks with DAPI and OS counterstaining using Agglutinin (*Agg*). *Scale bars*, 20 μm. *G*, transmission electron microscopy analysis of inner segments with ER cisternae encircled in *red* at 4 weeks of age. *Scale bars*, 200 nM. *INL*, inner nuclear layer.

Kinetics of Apoptosis in the Bbs12$^{-/-}$ Retina—Retinal degeneration was well underway by 4 weeks postnatally. By studying the developmental changes in the abundance apoptotic nuclei in *Bbs12*$^{+/+}$ and *Bbs12*$^{-/-}$ mice, we observed the first BBS12-dependent increase in cell death between postnatal days 12 and 14 (Fig. 5*A*). Furthermore, expression of *Caspase3*, *Caspase6*, *Caspase12*, *Bip*, and *Chop10* mRNAs was significantly up-regulated in *Bbs12*$^{-/-}$ retinas at postnatal day 14 (Fig. 5*B*), which correlated with an increase of BiP and CHOP10 protein contents in the *Bbs12*$^{-/-}$ retinas (Fig. 5*C* and supplemental Fig. S10). These data validate the *ex vivo* findings that ER stress is activated in BBS12-deprived retinas.

In Vivo Pharmacological Modulation of the UPR Slows Photoreceptor Loss Preserves Light Detection in Bbs12$^{-/-}$ Retinas—We next tried to protect *Bbs12*$^{-/-}$ retinas *in vivo* against apoptosis. Systemic treatment with VPA or GBZ in the drinking water did indeed have a positive effect on the retinal phenotype of the *Bbs12*$^{-/-}$ mice, because both systemic VPA and systemic GBZ administration mediated a thickening of the ONL (supplemental Fig. S12, *A* and *B*). Both treatments yielded an improvement of the light-detecting capacity of the photoreceptors, with an increased magnitude of the *a*-wave on ERG recordings (supplemental Fig. S12*D*). Interestingly, systemic VPA did not cause significant hepatic dysfunction in treated mice, as demonstrated by urea concentration in plasma,

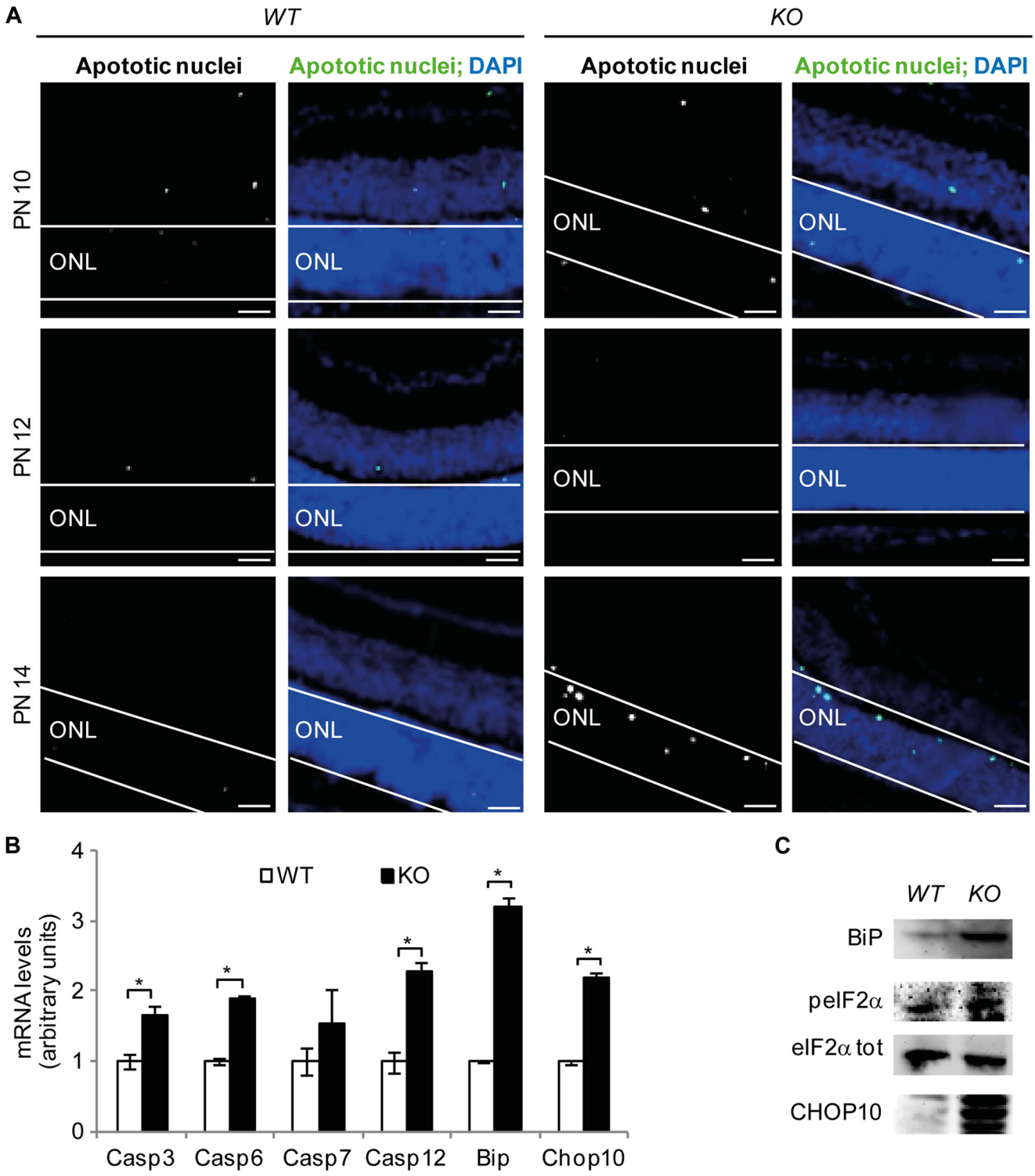

FIGURE 5. **Apoptosis in *Bbs12*$^{-/-}$ retina.** *A*, TUNEL assays in *WT and KO* retinas at postnatal days (*PN*) 10, 12, and 14. *Scale bars*, 30 μm. *B*, expression analysis of *Caspase3*, *-6*, *-7*, and *-12*, *Bip*, and *Chop10* in *WT* and *KO* retinas ($n = 3$). *, $p < 0.05$). *C*, immunodetection of BiP peIF2α, eIF2αtot, and CHOP10 in 2-week-old *WT* and *KO* retinas. See supplemental Fig. S10 for loading controls.

whereas systemic GBZ significantly did (supplemental Fig. S13). We therefore retained systemic administration for VPA but used a local eyedrop administration approach for both GBZ and the INH for our GIV*in* treatment. The INH oligopeptide cannot be administered orally. Furthermore, we did not try to inject the compounds because we did not want to risk an unexpected phenotype because of their antiapoptotic activity. GIV*in* treatment was able to protect the retina of Bbs12$^{-/-}$ mice substantially: the thickness of the ONL layer increased from ~33 μm in untreated *Bbs12*$^{-/-}$ animals to ~54 μm in GIV*in*-treated *Bbs12*$^{-/-}$ ones (Fig. 6, *A* and *B*). As in our *ex vivo* condition, GIV*in* increased the tissue concentration of BiP, peIF2α, and CHOP10 in *Bbs12*$^{+/+}$-treated animals (Fig. 6*C* and supplemental Fig. S11). In addition, Rhodopsin protein

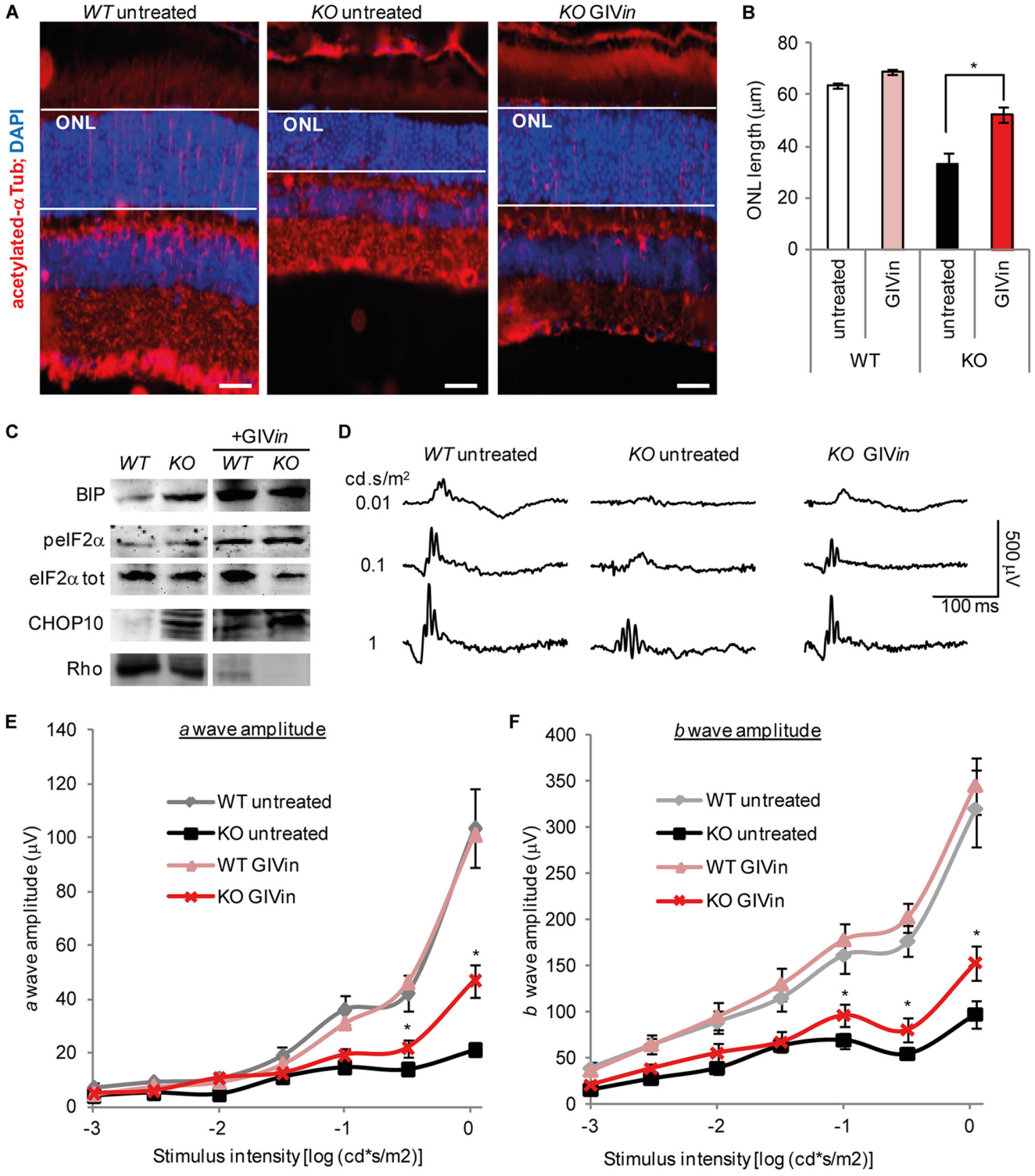

FIGURE 6. **Pharmacological modulation of UPR prevents photoreceptors loss in *Bbs12*$^{-/-}$ retina.** *A*, immunostaining of acetylated α-tubulin with DAPI counterstaining in indicated treated animals at 4 weeks of age. *Scale bars*, 20 μM. *B*, comparison of ONL length of GIV*in* treated and untreated mice at 4 weeks of age ($n = 6$). *, $p < 0.01$. *C*, immunodetection of BiP, peIF2α, eIF2αtot, CHOP10, and Rhodopsin in retinas from indicated treated 4-week-old animals. See supplemental Fig. S11 for loading controls and quantification. *D*, scotopic ERG recordings of animals with indicated treatment and genotype at 4 weeks of age. *E*, scotopic *a*-wave amplitude *versus* stimulus intensity (log) function of animals with indicated treatment and genotype at 4 weeks of age ($n = 12$). *, $p < 0.05$. *F*, scotopic *b*-wave amplitude *versus* stimulus intensity (log) function of indicated animals ($n = 12$). **, $p < 0.05$. The animals were treated for 2 weeks with GIV*in*: topical GBZ 7,5 μM + topical INH 500 μM + systemic VPA 5 mg/ml.

levels were decreased upon GIV*in* treatment, independently of the treated genotype (Fig. 6*C* and supplemental Fig. S11). This GIV*in*-mediated improvement of retinal thickness in the *Bbs12* KO corresponded with preservation of the amplitudes of *a*- and *b*-waves on ERGs (Fig. 6*D*). Indeed, we observed a ~2.7-fold increase in the amplitude of the *a*-wave (Fig. 6*E*) and a ~1.5-fold increase in that of the *b*-wave (Fig. 6*F*).

DISCUSSION

BBS is a ciliopathy characterized by an early onset of RP because of photoreceptor apoptosis. However, the precise cellular mechanisms leading to cell death are not known. Recently, tauroursodeoxycholic acid was reported to have beneficial effects on the retinal phenotype of the *Bbs1*$^{M390R/M390R}$ mouse (37). Tauroursodeoxycholic acid was described in that study as having an antiapoptotic effect inducing retinal thickening in treated animals, but its exact apoptotic mechanism has so far remain undetermined. In this study, we integrated *ex vivo* and *in vivo* approaches to dissect the mechanism involved in retinal degeneration in the absence of one of the BBS members, namely BBS12. The latter impaired the ciliary trafficking of key photoreceptor proteins and caused photoreceptor cell death through prolonged UPR activation. Based on these findings, we defined the GIV*in* treatment, which resulted in a substantial protection of the photoreceptors against apoptosis and maintained the ability to detect light *in vivo*.

PERK-mediated Branch of the UPR Drives Apoptosis in BBS12-deprived Photoreceptors—This protein overload in the IS induced an accumulation of proteins inside the ER lumen, as reflected by the characteristic swelling of the ER cisternae (Fig. 4*G*). An unbalance between the amounts of *de novo* synthesized proteins and the amount of the BiP chaperone residing in the ER causes ER stress and activates the UPR pathway. In the BBS12-deprived photoreceptors, the UPR was characterized by increased BiP, Caspase12, and peIF2α tissue levels. The three main cellular stress transducers (IRE1, PERK, and ATF6 (15)) have different temporal patterns of activation during the UPR signaling cascade (20). IRE1 was activated in absence of BBS12, because we could detect the stress-induced splice variant of *Xbp1*. Nevertheless, this branch was not selected as a pharmacological target because it does not induce apoptosis during ER stress but instead regulates lipogenesis and ER-associated protein degradation (38). The transcription factor ATF6 regulates the expression of UPR genes, such as BiP, to increase ER folding capacity and expression of ER-associated protein degradation genes to ameliorate protein overload (39) but is not involved in cell death (40). The PERK-dependent branch of the UPR, on the other hand, is proapoptotic for cells submitted to pertinacious ER stress (41). Our results confirmed that PERK activity was required to launch the apoptotic cascade in the absence of BBS12 and highlight that the PERK branch is the UPR branch that drives apoptosis in BBS12-depleted photoreceptors.

Efficient Decrease of Overall Cellular Protein Load in BBS12-deprived Photoreceptors Protects against Apoptosis and Preserved Light Detection—With prolonged protein overload leading to apoptosis of the BBS12-deprived photoreceptors, decreasing protein load by either degrading the newly synthesized proteins or preventing their biosynthesis represents interesting therapeutic avenues. In this respect, VPA is known to modulate transcription and activity of BiP, a resident ER chaperone (35), and is already being used as a neuroprotective agent in retinal diseases (42). VPA protects, for example, retinal cells in the rat against apoptosis that is induced by ischemia-reperfusion injury by increasing BiP expression and reducing Caspase12 activation (43). In BBS12-deprived retinal explants, VPA treatment induced a significant increase of BiP protein level and reduction in apoptosis. Interestingly, *Bip* mRNA level was lower in *Bbs12*-depleted explants treated with VPA than in *Bbs12*-depleted retinal explants without VPA treatment, although this level was higher than the sh*Ctl* explants without pharmacological treatment. This is probably correlated with the known uncorrelated rates between *Bip* transcription and translation (44). Consistent with the fact that increasing the BiP/nascent proteins ratio in the ER favored unfolded proteins degradation, hence decreasing overall cellular protein load (45), mice treated with VPA alone (supplemental Fig. S12*C*) showed decrease Rhodopsin protein content. This effect was associated with increased ONL thickness and improved ERG recordings (supplemental Fig. S12, *B* and *D*). Apart from being a historical drug used to treat epilepsy in human patients (46), VPA was recently used in a trial of retinitis pigmentosa patients with mutations in the Rhodopsin gene (47–49). Although VPA-treated patients had a larger visual field than untreated patients in the first study, controversy arose because of inefficiency for other patients and a lack of mechanistic insight on how the VPA protected against apoptosis. Our results contribute to clarifying the underlying mechanism of the beneficial outcome observed in a subset of RP patients.

The second approach to prevent deleterious protein overload is to maintain high levels of peIF2α, thereby inhibiting CAP-dependent translation (50). We opted to inhibit the dephosphorylation of peIF2α using GBZ, a specific inhibitor of the eIF2α-phosphatase, GADD34 (36). GBZ bears anti-prion activity (34) and was used to cure diseases linked to unfolded proteins conditions (51). Efficacy in reducing protein load in the photoreceptor was successfully demonstrated in the *Ahi1*$^{-/-}$ mouse (14). Loss of the ciliary protein AHI1 causes retinitis pigmentosa in mice and retinal degeneration in humans suffering from some variants of Joubert syndrome, another ciliopathy. In our studies, GBZ specifically increased peIF2α and CHOP10 protein levels. CHOP10 is associated with both pro- and antiapoptotic activities (52, 53), but our study demonstrates that GBZ-mediated CHOP10 increase is mainly antiapoptotic in BBS-deprived photoreceptors. Moreover, as for VPA, the beneficial effect of GBZ was associated with decreased protein load as demonstrated by the significant reduction of Rhodopsin protein levels (supplemental Figs. S12*C* and S14). There is a reduced Rhodopsin load that is presumably in good shape and correctly located in the treated mice, whereas in untreated mice, Rhodopsin is aggregated in the IS and not functional. In aggregate, these findings clearly demonstrate that it is a protein accumulation inside the IS of the BBS-deficient photoreceptors that triggers apoptosis and that pharmacological reduction of this protein overload has a major beneficial effect.

Simultaneous Increase of ER-resident Chaperone BiP Activity, Inhibition of CAP-dependent Translation, and Inactivation of Caspase12 Activity Represent the Most Efficient Way to Maintain Photoreceptors—Although substantial protection was obtained against apoptosis with either VPA or GBZ or both (supplemental Fig. S8), there was still a significant increase in apoptotic nuclei in absence of BBS12 in these treated photoreceptors. Even though we could measure a substantial decrease in Rhodopsin, the most abundant photoreceptor protein, in the treated BBS12-deperived photoreceptors, the maintained significant apoptotic activity indicated residual UPR activation. In an attempt to optimize our protective treatment, we tested a

third pharmacological approach based on the UPR-specific Caspase12 inhibition (54, 55). Used alone, the Caspase12 inhibitor INH was ~20% less efficient in preventing apoptosis than VPA or GBZ (Fig. 3), even if it unexpectedly impacted the peIF2α and CHOP10 levels but not BiP expression levels. Interestingly, GIV, combining the three molecules, was the most efficient way to decrease apoptotic levels both *ex vivo* and *in vivo*. This result could be associated with the synergistic up-regulation of the three targets, namely BiP, peIF2α, and CHO10 (Fig. 3*F*).

GIV Treatment, Other BBS Proteins, and Time of Administration—In this study, we showed that the efficient modulation of the UPR induced by a defect in ICT in BBS12-deprived photoreceptors allows successful slow down of photoreceptor apoptosis. Our finding is strengthened by the previously used tauroursodeoxycholic acid treatment in the *Bbs1* mutated mice because it is a detergent and chemical chaperone that enhances the adaptive capacity of the ER in UPR conditions (56, 57). These results demonstrate that the proapoptotic mechanism is similar in both cases and that GIV can most probably be extrapolated to all known BBS proteins as they all interact together (58). Interestingly, the first detectable apoptotic responses developed between postnatal days 12 and 14, that is, when photoreceptors have differentiated and matured (59). These data therefore indicate that BBS12 protein is not required for the maturation process of the photoreceptors but becomes essential for photoreceptor function. We show that pharmacological treatment can therefore be administered once the photoreceptors are functionally detecting light stimulus.

Conclusion—The identification of the precise UPR mechanism and the optimized GIV treatment represent an efficient strategy in preserving vision in the studied model with possible extension to patients. This pharmacological treatment could potentially be extended to the other ciliopathies, once proven that they share similar UPR proapoptotic mechanisms. However, this pharmacological treatment should not be considered as a long term curative treatment such as gene therapy. In fact, both techniques are complementary, because the pharmacological approach aims to preserve the maximum number of healthy photoreceptor cells preparing for gene therapy. Pharmacological dynamics, toxicity studies, and applicability to human beings are the next steps following this work pointing to precise targets for preventing retinal degeneration in ciliopathies.

Acknowledgments—We thank RETINA France, UNADEV, Fondation de France, and the patient associations for support. We thank the Institut Clinique de la Souris for the generation of the Bbs12 mouse model, Michel Roux for the lending of the ERG device, and UMR748 employees for the mice breeding.

REFERENCES

1. Mockel, A., Perdomo, Y., Stutzmann, F., Letsch, J., Marion, V., and Dollfus, H. (2011) Retinal dystrophy in Bardet-Biedl syndrome and related syndromic ciliopathies. *Prog. Retin. Eye Res.* **30,** 258–274
2. Badano, J. L., Mitsuma, N., Beales, P. L., and Katsanis, N. (2006) The ciliopathies. An emerging class of human genetic disorders. *Annu. Rev. Genomics Hum. Genet.* **7,** 125–148
3. Marion, V., Stutzmann, F., Gérard, M., De Melo, C., Schaefer, E., Claussmann, A., Hellé, S., Delague, V., Souied, E., Barrey, C., Verloes, A., Stoetzel, C., and Dollfus, H. (2012) Exome sequencing identifies mutations in LZTFL1, a BBSome and smoothened trafficking regulator, in a family with Bardet-Biedl syndrome with situs inversus and insertional polydactyly. *J. Med. Genet.* **49,** 317–321
4. Fliegauf, M., Benzing, T., and Omran, H. (2007) When cilia go bad. Cilia defects and ciliopathies. *Nat. Rev. Mol. Cell Biol.* **8,** 880–893
5. Nachury, M. V., Loktev, A. V., Zhang, Q., Westlake, C. J., Peränen, J., Merdes, A., Slusarski, D. C., Scheller, R. H., Bazan, J. F., Sheffield, V. C., and Jackson, P. K. (2007) A core complex of BBS proteins cooperates with the GTPase Rab8 to promote ciliary membrane biogenesis. *Cell* **129,** 1201–1213
6. Seo, S., Baye, L. M., Schulz, N. P., Beck, J. S., Zhang, Q., Slusarski, D. C., and Sheffield, V. C. (2010) BBS6, BBS10, and BBS12 form a complex with CCT/TRiC family chaperonins and mediate BBSome assembly. *Proc. Natl. Acad. Sci. U.S.A.* **107,** 1488–1493
7. Abd-El-Barr, M. M., Sykoudis, K., Andrabi, S., Eichers, E. R., Pennesi, M. E., Tan, P. L., Wilson, J. H., Katsanis, N., Lupski, J. R., and Wu, S. M. (2007) Impaired photoreceptor protein transport and synaptic transmission in a mouse model of Bardet-Biedl syndrome. *Vision Res.* **47,** 3394–3407
8. Fath, M. A., Mullins, R. F., Searby, C., Nishimura, D. Y., Wei, J., Rahmouni, K., Davis, R. E., Tayeh, M. K., Andrews, M., Yang, B., Sigmund, C. D., Stone, E. M., and Sheffield, V. C. (2005) Mkks-null mice have a phenotype resembling Bardet-Biedl syndrome. *Hum. Mol. Genet.* **14,** 1109–1118
9. Nishimura, D. Y., Fath, M., Mullins, R. F., Searby, C., Andrews, M., Davis, R., Andorf, J. L., Mykytyn, K., Swiderski, R. E., Yang, B., Carmi, R., Stone, E. M., and Sheffield, V. C. (2004) Bbs2-null mice have neurosensory deficits, a defect in social dominance, and retinopathy associated with mislocalization of rhodopsin. *Proc. Natl. Acad. Sci. U.S.A.* **101,** 16588–16593
10. Mykytyn, K., Mullins, R. F., Andrews, M., Chiang, A. P., Swiderski, R. E., Yang, B., Braun, T., Casavant, T., Stone, E. M., and Sheffield, V. C. (2004) Bardet-Biedl syndrome type 4 (BBS4)-null mice implicate Bbs4 in flagella formation but not global cilia assembly. *Proc. Natl. Acad. Sci. U.S.A.* **101,** 8664–8669
11. Davis, R. E., Swiderski, R. E., Rahmouni, K., Nishimura, D. Y., Mullins, R. F., Agassandian, K., Philp, A. R., Searby, C. C., Andrews, M. P., Thompson, S., Berry, C. J., Thedens, D. R., Yang, B., Weiss, R. M., Cassell, M. D., Stone, E. M., and Sheffield, V. C. (2007) A knockin mouse model of the Bardet-Biedl syndrome 1 M390R mutation has cilia defects, ventriculomegaly, retinopathy, and obesity. *Proc. Natl. Acad. Sci. U.S.A.* **104,** 19422–19427
12. Pretorius, P. R., Baye, L. M., Nishimura, D. Y., Searby, C. C., Bugge, K., Yang, B., Mullins, R. F., Stone, E. M., Sheffield, V. C., and Slusarski, D. C. (2010) Identification and functional analysis of the vision-specific BBS3 (ARL6) long isoform. *PLoS Genet.* **6,** e1000884
13. Tam, B. M., and Moritz, O. L. (2006) Characterization of rhodopsin P23H-induced retinal degeneration in a *Xenopus laevis* model of retinitis pigmentosa. *Invest. Ophthalmol. Vis. Sci.* **47,** 3234–3241
14. Louie, C. M., Caridi, G., Lopes, V. S., Brancati, F., Kispert, A., Lancaster, M. A., Schlossman, A. M., Otto, E. A., Leitges, M., Gröne, H. J., Lopez, I., Gudiseva, H. V., O'Toole, J. F., Vallespin, E., Ayyagari, R., Ayuso, C., Cremers, F. P., den Hollander, A. I., Koenekoop, R. K., Dallapiccola, B., Ghiggeri, G. M., Hildebrandt, F., Valente, E. M., Williams, D. S., and Gleeson, J. G. (2010) AHI1 is required for photoreceptor outer segment development and is a modifier for retinal degeneration in nephronophthisis. *Nat. Genet.* **42,** 175–180
15. Ron, D., and Walter, P. (2007) Signal integration in the endoplasmic reticulum unfolded protein response. *Nat. Rev. Mol. Cell Biol.* **8,** 519–529
16. Griciuc, A., Aron, L., and Ueffing, M. (2011) ER stress in retinal degeneration. A target for rational therapy? *Trends Mol. Med.* **17,** 442–451
17. Yang, L. P., Wu, L. M., Guo, X. J., and Tso, M. O. (2007) Activation of endoplasmic reticulum stress in degenerating photoreceptors of the *rd1* mouse. *Invest. Ophthalmol. Vis. Sci.* **48,** 5191–5198
18. Chiang, W. C., Messah, C., and Lin, J. H. (2012) IRE1 directs proteasomal and lysosomal degradation of misfolded rhodopsin. *Mol. Biol. Cell* **23,** 758–770
19. Shinde, V. M., Sizova, O. S., Lin, J. H., LaVail, M. M., and Gorbatyuk, M. S. (2012) ER stress in retinal degeneration in S334ter Rho rats. *PLoS One* **7,** e33266
20. Lin, J. H., Li, H., Yasumura, D., Cohen, H. R., Zhang, C., Panning, B., Shokat, K. M., Lavail, M. M., and Walter, P. (2007) IRE1 signaling affects cell fate during the unfolded protein response. *Science* **318,** 944–949
21. Mendes, H. F., and Cheetham, M. E. (2008) Pharmacological manipulation of gain-of-function and dominant-negative mechanisms in rhodopsin retinitis pigmentosa. *Hum. Mol. Genet.* **17,** 3043–3054

22. Gorbatyuk, M. S., Knox, T., LaVail, M. M., Gorbatyuk, O. S., Noorwez, S. M., Hauswirth, W. W., Lin, J. H., Muzyczka, N., and Lewin, A. S. (2010) Restoration of visual function in P23H rhodopsin transgenic rats by gene delivery of BiP/Grp78. *Proc. Natl. Acad. Sci. U.S.A.* **107,** 5961–5966
23. Reidel, B., Orisme, W., Goldmann, T., Smith, W. C., and Wolfrum, U. (2006) Photoreceptor vitality in organotypic cultures of mature vertebrate retinas validated by light-dependent molecular movements. *Vision Res.* **46,** 4464–4471
24. Harrison, D. C., Medhurst, A. D., Bond, B. C., Campbell, C. A., Davis, R. P., and Philpott, K. L. (2000) The use of quantitative RT-PCR to measure mRNA expression in a rat model of focal ischemia. Caspase-3 as a case study. *Brain Res. Mol. Brain Res.* **75,** 143–149
25. Li, P., Nijhawan, D., Budihardjo, I., Srinivasula, S. M., Ahmad, M., Alnemri, E. S., and Wang, X. (1997) Cytochrome *c* and dATP-dependent formation of Apaf-1/caspase-9 complex initiates an apoptotic protease cascade. *Cell* **91,** 479–489
26. Aoyama, K., Burns, D. M., Suh, S. W., Garnier, P., Matsumori, Y., Shiina, H., and Swanson, R. A. (2005) Acidosis causes endoplasmic reticulum stress and caspase-12-mediated astrocyte death. *J. Cereb. Blood Flow Metab.* **25,** 358–370
27. Katayama, T., Imaizumi, K., Sato, N., Miyoshi, K., Kudo, T., Hitomi, J., Morihara, T., Yoneda, T., Gomi, F., Mori, Y., Nakano, Y., Takeda, J., Tsuda, T., Itoyama, Y., Murayama, O., Takashima, A., St George-Hyslop, P., Takeda, M., and Tohyama, M. (1999) Presenilin-1 mutations downregulate the signalling pathway of the unfolded-protein response. *Nat. Cell Biol.* **1,** 479–485
28. Tabas, I., and Ron, D. (2011) Integrating the mechanisms of apoptosis induced by endoplasmic reticulum stress. *Nat. Cell Biol.* **13,** 184–190
29. Yoshida, H., Matsui, T., Yamamoto, A., Okada, T., and Mori, K. (2001) XBP1 mRNA is induced by ATF6 and spliced by IRE1 in response to ER stress to produce a highly active transcription factor. *Cell* **107,** 881–891
30. Harding, H. P., Zhang, Y., and Ron, D. (1999) Protein translation and folding are coupled by an endoplasmic-reticulum-resident kinase. *Nature* **397,** 271–274
31. Harding, H. P., Novoa, I., Zhang, Y., Zeng, H., Wek, R., Schapira, M., and Ron, D. (2000) Regulated translation initiation controls stress-induced gene expression in mammalian cells. *Mol. Cell* **6,** 1099–1108
32. Berlanga, J. J., Herrero, S., and de Haro, C. (1998) Characterization of the hemin-sensitive eukaryotic initiation factor 2α kinase from mouse nonerythroid cells. *J. Biol. Chem.* **273,** 32340–32346
33. Lu, J., O'Hara, E. B., Trieselmann, B. A., Romano, P. R., and Dever, T. E. (1999) The interferon-induced double-stranded RNA-activated protein kinase PKR will phosphorylate serine, threonine, or tyrosine at residue 51 in eukaryotic initiation factor 2α. *J. Biol. Chem.* **274,** 32198–32203
34. Tribouillard-Tanvier, D., Béringue, V., Desban, N., Gug, F., Bach, S., Voisset, C., Galons, H., Laude, H., Vilette, D., and Blondel, M. (2008) Antihypertensive drug guanabenz is active *in vivo* against both yeast and mammalian prions. *PLoS One* **3,** e1981
35. Wang, J. F., Bown, C., and Young, L. T. (1999) Differential display PCR reveals novel targets for the mood-stabilizing drug valproate including the molecular chaperone GRP78. *Mol. Pharmacol.* **55,** 521–527
36. Tsaytler, P., Harding, H. P., Ron, D., and Bertolotti, A. (2011) Selective inhibition of a regulatory subunit of protein phosphatase 1 restores proteostasis. *Science* **332,** 91–94
37. Drack, A. V., Dumitrescu, A. V., Bhattarai, S., Gratie, D., Stone, E. M., Mullins, R., and Sheffield, V. C. (2012) TUDCA slows retinal degeneration in two different mouse models of retinitis pigmentosa and prevents obesity in Bardet-Biedl syndrome type 1 mice. *Invest. Ophthalmol. Vis. Sci.* **53,** 100–106
38. Reimold, A. M., Iwakoshi, N. N., Manis, J., Vallabhajosyula, P., Szomolanyi-Tsuda, E., Gravallese, E. M., Friend, D., Grusby, M. J., Alt, F., and Glimcher, L. H. (2001) Plasma cell differentiation requires the transcription factor XBP-1. *Nature* **412,** 300–307
39. Kaneko, M., and Nomura, Y. (2003) ER signaling in unfolded protein response. *Life Sci.* **74,** 199–205
40. Yamamoto, K., Sato, T., Matsui, T., Sato, M., Okada, T., Yoshida, H., Harada, A., and Mori, K. (2007) Transcriptional induction of mammalian ER quality control proteins is mediated by single or combined action of ATF6α and XBP1. *Dev. Cell* **13,** 365–376
41. Lin, J. H., Li, H., Zhang, Y., Ron, D., and Walter, P. (2009) Divergent effects of PERK and IRE1 signaling on cell viability. *PLoS One* **4,** e4170
42. Biermann, J., Grieshaber, P., Goebel, U., Martin, G., Thanos, S., Di Giovanni, S., and Lagreze, W. A. (2010) Valproic acid-mediated neuroprotection and regeneration in injured retinal ganglion cells. *Invest. Ophthalmol. Vis. Sci.* **51,** 526–534
43. Zhang, Z., Tong, N., Gong, Y., Qiu, Q., Yin, L., Lv, X., and Wu, X. (2011) Valproate protects the retina from endoplasmic reticulum stress-induced apoptosis after ischemia-reperfusion injury. *Neurosci. Lett.* **504,** 88–92
44. Rutkowski, D. T., Arnold, S. M., Miller, C. N., Wu, J., Li, J., Gunnison, K. M., Mori, K., Sadighi Akha, A. A., Raden, D., and Kaufman, R. J. (2006) Adaptation to ER stress is mediated by differential stabilities of pro-survival and pro-apoptotic mRNAs and proteins. *PLoS Biol.* **4,** e374
45. Ushioda, R., Hoseki, J., Araki, K., Jansen, G., Thomas, D. Y., and Nagata, K. (2008) ERdj5 is required as a disulfide reductase for degradation of misfolded proteins in the ER. *Science* **321,** 569–572
46. Chateauvieux, S., Morceau, F., Dicato, M., and Diederich, M. (2010) Molecular and therapeutic potential and toxicity of valproic acid. *J. Biomed. Biotechnol.* **2010,** 479364
47. Clemson, C. M., Tzekov, R., Krebs, M., Checchi, J. M., Bigelow, C., and Kaushal, S. (2011) Therapeutic potential of valproic acid for retinitis pigmentosa. *Br J. Ophthalmol.* **95,** 89–93
48. Sandberg, M. A., Rosner, B., Weigel-DiFranco, C., and Berson, E. L. (2011) Lack of scientific rationale for use of valproic acid for retinitis pigmentosa. *Br. J. Ophthalmol.* **95,** 744
49. van Schooneveld, M. J., van den Born, L. I., van Genderen, M., and Bollemeijer, J. G. (2011) The conclusions of Clemson et al. concerning valproic acid are premature. *Br. J. Ophthalmol.* **95,** 153; author reply 153–154
50. Fernandez, J., Yaman, I., Sarnow, P., Snider, M. D., and Hatzoglou, M. (2002) Regulation of internal ribosomal entry site-mediated translation by phosphorylation of the translation initiation factor eIF2α. *J. Biol. Chem.* **277,** 19198–19205
51. Barbezier, N., Chartier, A., Bidet, Y., Buttstedt, A., Voisset, C., Galons, H., Blondel, M., Schwarz, E., and Simonelig, M. (2011) Antiprion drugs 6-aminophenanthridine and guanabenz reduce PABPN1 toxicity and aggregation in oculopharyngeal muscular dystrophy. *EMBO Mol. Med.* **3,** 35–49
52. Halterman, M. W., Gill, M., DeJesus, C., Ogihara, M., Schor, N. F., and Federoff, H. J. (2010) The endoplasmic reticulum stress response factor CHOP-10 protects against hypoxia-induced neuronal death. *J. Biol. Chem.* **285,** 21329–21340
53. Skalet, A. H., Isler, J. A., King, L. B., Harding, H. P., Ron, D., and Monroe, J. G. (2005) Rapid B cell receptor-induced unfolded protein response in nonsecretory B cells correlates with pro- *versus* antiapoptotic cell fate. *J. Biol. Chem.* **280,** 39762–39771
54. Balan, A. G., Myers, B. J., Maganti, J. L., and Moore, D. B. (2010) ER-targeted Bcl-2 and inhibition of ER-associated caspase-12 rescue cultured immortalized cells from ethanol toxicity. *Alcohol* **44,** 553–563
55. Dalal, S., Foster, C. R., Das, B. C., Singh, M., and Singh, K. (2012) B-adrenergic receptor stimulation induces endoplasmic reticulum stress in adult cardiac myocytes. Role in apoptosis. *Mol. Cell Biochem.* **364,** 59–70
56. de Almeida, S. F., Picarote, G., Fleming, J. V., Carmo-Fonseca, M., Azevedo, J. E., and de Sousa, M. (2007) Chemical chaperones reduce endoplasmic reticulum stress and prevent mutant HFE aggregate formation. *J. Biol. Chem.* **282,** 27905–27912
57. Ozcan, U., Yilmaz, E., Ozcan, L., Furuhashi, M., Vaillancourt, E., Smith, R. O., Görgün, C. Z., and Hotamisligil, G. S. (2006) Chemical chaperones reduce ER stress and restore glucose homeostasis in a mouse model of type 2 diabetes. *Science* **313,** 1137–1140
58. Zhang, Q., Yu, D., Seo, S., Stone, E. M., and Sheffield, V. C. (2012) Intrinsic protein-protein interaction-mediated and chaperonin-assisted sequential assembly of stable bardet-biedl syndrome protein complex, the BBSome. *J. Biol. Chem.* **287,** 20625–20635
59. Sedmak, T., and Wolfrum, U. (2011) Intraflagellar transport proteins in ciliogenesis of photoreceptor cells. *Biol. Cell* **103,** 449–466
60. Marion, V., Mockel, A., De Melo, C., Obringer, C., Claussmann, A., Simon, A., Messaddeq, N., Durand, M., Dupuis, L., Loeffler, J. P., King, P., Mutter-Schmidt, C., Petrovsky, N., Stoetzel, C., and Dollfus, H. (2012) *Cell Metab.* **16,** 363–377